Solubility of nonpolar solutes in water: Computer simulations using the CF1 central force model

Jonathan W. Arthur and A. D. J. Haymet

Citation: The Journal of Chemical Physics **109**, 7991 (1998); doi: 10.1063/1.477446
View online: http://dx.doi.org/10.1063/1.477446
View Table of Contents: http://scitation.aip.org/content/aip/journal/jcp/109/18?ver=pdfcov
Published by the AIP Publishing

Solubility of nonpolar solutes in water: Computer simulations using the CF1 central force model

Jonathan W. Arthur
School of Chemistry, University of Sydney, NSW 2006 Australia

A. D. J. Haymet[a)]
Department of Chemistry, University of Houston, Houston, Texas 77204

(Received 3 June 1998; accepted 28 July 1998)

Nonpolar solutes in water are modeled by the CF1 central force model for the water-water interactions and a shifted-force Lennard-Jones potential function for the solute-water interactions. Thermodynamic integration is used to calculate the solvation free energy of solutes of various sizes. A systematic exploration of the effect of the size of the solute and the depth of the potential well is carried out. This allows an examination of the change in the solvation free energy as the solute size and potential well depth are independently varied. The solvation free energies of the noble gas series are also studied. The results compare favorably with experiment and previous studies, indicating the suitability of the CF1 model of water for use in free energy calculations. An information theory approximation is used to calculate the solvation free energy for hard spheres of various sizes from a simulation of pure CF1 water. The results of this approximation show trends similar to the results of our simulations using the modified shifted-force potentials. © *1998 American Institute of Physics.* [S0021-9606(98)51141-5]

I. INTRODUCTION

The computer simulation techniques of molecular dynamics[1] and Monte Carlo[2] are now useful for making accurate calculations of various experimental quantities in the study of solvation. The development of the statistical mechanical techniques of free energy perturbation (FEP)[3–8] and thermodynamic integration (TI)[3,7,9,10] are especially relevant to this work. These techniques, together with the power of molecular dynamics and Monte Carlo simulations, allow the accurate determination of free energy differences for many systems of interest.

Free energy calculations have been used over the years to study the processes involved in solvation.[4,6,9,11–16] One phenomenon that has received a great deal of attention is the hydrophobic effect.[11,12,17–31] It is claimed that hydrophobicity plays a role in numerous solvation processes including the immiscibility of nonpolar substances with water,[32] the folding of biological macromolecules in water,[33] micelle and membrane formation and stability,[34,35] clathrate hydrate formation,[36] and the binding of a drug to its receptor.[37] There are two distinct aspects to hydrophobicity.[21] The first is termed hydrophobic hydration: it describes the interaction of a nonpolar solute with water and the effect of the nonpolar solute on the structure of the surrounding water. The second is called hydrophobic interaction, and deals with the solvent-induced forces existing between two or more hydrophobic species in a water solvent. This paper deals specifically with hydrophobic hydration.

In this work we build upon previous studies by determining the effect of changing the size of a solute on the free energy of solvation while the depth of the potential well is kept constant. Similarly we examine the effect of changing the potential well depth at constant solute size. We also study the effect of using the flexible CF1 model of water on the thermodynamic properties of solvation of nonpolar solutes. In Sec. II we review earlier calculations. Section III of this paper briefly describes the theory of free energy calculations and the potentials used in the simulations. The technique of thermodynamic integration is described thoroughly and the modified shifted-force potentials are introduced. Section IV sets out the details of the molecular dynamics simulations. The results and discussion are presented in Sec. V and conclusions are drawn in Sec. VI.

II. BRIEF REVIEW OF SIMULATIONS AND STUDIES OF HYDROPHOBICITY

Several earlier studies have examined the effect of changing solute size on the solvation of nonpolar solutes in water. A comprehensive review of the literature has been given by Blokzijl and Engberts,[38] and only a brief review of the effect of solute size on solvation is given here.

Okazaki *et al.*[17] studied the effect of solute size on the internal energy of solutes in water in an early contribution to this field of study. They examined the structure of water around the solute and showed that the structure does not change monotonically with the size of the solute. The effect of temperature on the hydrophobic hydration of nonpolar solutes was analyzed by Okazaki *et al.*[18] Swope and Andersen[19] studied the solubility of gases in liquid water. They performed a more systematic study varying the solute size, potential well depth, and temperature in their calculations. Pearlman and Kollman[5] calculated the free energies of solvation for the noble gas series (neon, krypton and xenon)

[a)]Author to whom correspondence should be addressed.

and methane. Similar calculations have been performed by Guillot *et al.*[11,12] and Straatsma *et al.*[39] The results of the three groups are reasonably consistent with each other and experiment, at least for the smaller solutes. Lazaridis and Paulaitis[22] studied the effect of solute size on various components of the entropy of solvation for the full noble gas series (helium to radon). They found the solute size to be the primary factor determining the entropy of solvation. Perkyns and Pettitt[40] used integral equation approximations to calculate the chemical potential of a Lennard-Jones sphere in water over a range of solute sizes and temperature/pressure states. They concluded that the chemical potential is predominantly entropic in nature.

High temperature and pressure studies on the effect of solute size have been carried out by Lin and Wood[14] using a homologous series of alkanes; again, the diameter of the water-alkane interaction was found to be the most important parameter. Similar solvation studies have also explored the importance of solute size in ionic systems. Straatsma and Berendsen[9] studied the hydration of ions of various sizes and a theoretical treatment of the solvation of ions has been developed by Hummer *et al.*[41] Recent studies of particular interest include the work of Lynden-Bell and Rasaiah,[15] who used an extended Lagrangian methodology to consider the charge and solute size as dynamic variables. This allows various thermodynamic properties to be determined as functions of the solute size and charge. Another recent development is the use of information theory techniques to calculate the free energy of hydration of hard sphere solutes using information on cavity formation in liquid water.[42–44] This technique presents an elegant and simple approximation for determining free energies.

In many of these previous studies, the effect of solute size on solubility is coupled to the strength of the potential of interaction or the shape of the molecule. In particular, the studies often focus on a homologous series of either alkanes or noble gases. In moving from one species in this series to the next, two parameters change simultaneously, the solute size and the depth of the potential well of interaction between the solute and the water. Thus plots of the variation of thermodynamic quantities (such as the free energy of solvation) as a function of solute size often have an implicit change in the solute-water interaction potential. It is desirable to assess the effect of changing the solute size *independently* of the well depth. Many of the previous studies are also performed using rigid models of water such as SPC, TIP4P or TIP3P.[45] While these models accurately reproduce various experimental quantities[21,45,46] of liquid water they do not consider the effect of the vibrational modes of a water molecule. Part of this study examines the effect of using a flexible model of water on the various thermodynamic properties.

III. CALCULATION OF THE FREE ENERGY

A. Thermodynamic integration

The determination of free energy differences is based on classical statistical mechanical principles.[47] The two common methods for calculating the free energy difference between two states are free energy perturbation and thermodynamic integration. It is generally accepted that perturbation theory provides accurate estimates of the free energy differences for systems differing only slightly in their structure. However, the technique of thermodynamic integration is accepted as the more accurate method for systems where the two states are significantly different.[3] A recent review of various techniques for calculating the free energy of solvation also suggests that thermodynamic integration is the most reliable approach.[48]

In the thermodynamic integration method the system progresses from an initial state to a final state representing the two systems for which a free energy difference is desired. The two states are each specified by a set of intramolecular and intermolecular potentials. To calculate the free energy difference between these two states, the system must gradually change from the initial state to the final state. The path taken by the system during this change or ''mutation'' between states is determined by a parameter, λ, known as the coupling parameter. The coupling parameter takes values between 0 and 1 with the final and initial states of the system defined by these two values, respectively. As λ varies from 1 to 0 (or equivalently from 0 to 1), the mutation proceeds from the initial state to the final state. The pathway defined by this coordinate can be a true reaction coordinate or a hypothetical one. The methodology developed here is for the isothermal-isobaric (NPT) ensemble, however, the formulation for the canonical ensemble is analogous.[7,49]

The Hamiltonian and the partition function for the system are functions of the coupling parameter λ. The partition function for the system is

$$\Xi(\lambda)=\frac{1}{h^{3N}N!}\int\int\int dV d\mathbf{p}^N d\mathbf{q}^N \exp\left\{-\frac{H(\lambda)+pV}{k_BT}\right\}, \tag{1}$$

where N is the number of particles, h is Planck's constant, $H(\lambda)$ is the Hamiltonian that is dependent on the progression along the reaction coordinate, p is the pressure, V is the volume, k_B is the Boltzmann constant, T is the absolute temperature and $\mathbf{p}^N$ and $\mathbf{q}^N$ are the momenta and positions of the N particles.

The Gibbs free energy of the system is then given by

$$G(\lambda)=-k_BT\ln\Xi(\lambda). \tag{2}$$

Differentiating this quantity with respect to λ then gives

$$\frac{\partial G(\lambda)}{\partial\lambda}=-\frac{k_BT}{\Xi(\lambda)}\left[\frac{\partial\Xi(\lambda)}{\partial\lambda}\right]=\left\langle\frac{\partial H(\lambda)}{\partial\lambda}\right\rangle_\lambda. \tag{3}$$

This last quantity is an ensemble average measured during the simulations.

The Gibbs free energy is obtained by integration of Eq. (3),

$$\Delta G=\int_0^1\left[\frac{\partial G(\lambda)}{\partial\lambda}\right]d\lambda=\int_0^1\left\langle\frac{\partial H(\lambda)}{\partial\lambda}\right\rangle_\lambda d\lambda. \tag{4}$$

This integral is calculated by replacing the integration with a finite sum. In this work the Gauss-Legendre integration technique is used. This replaces the integral by a weighted sum,

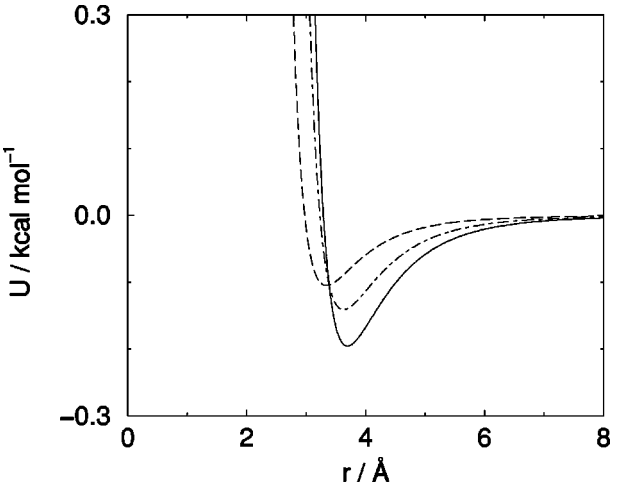

FIG. 1. Potential curves used in studying the ''mutation'' of neon into argon. The solid line is a Lennard-Jones potential representing the interaction of an argon atom and the oxygen atom on a water molecule. The dashed line is the analogous neon-oxygen potential. The dot-dashed line represents the potential of interaction between the particles at some intermediate point λ_j given by the linear combination in Eq. (6).

$$\int_0^1 \left\langle \frac{\partial H(\lambda)}{\partial \lambda} \right\rangle_\lambda d\lambda = \sum_{i=1}^{n} w_i \left\langle \frac{\partial H(\lambda)}{\partial \lambda} \right\rangle_{\lambda_i}, \tag{5}$$

where w_i are the usual weights.[50] The values of λ_i are predetermined by the Gauss-Legendre integration technique. Improvements in the calculation of the sum can be made by using higher-order Gauss-Legendre integrations involving simulations at more points along the progression from $\lambda = 1$ to 0. This improvement in the quality of the integration needs to be balanced against the extra simulation time required.

The theoretical methodology described in the previous section can be elucidated through a particular example. Consider a single nonpolar solute in water, where the free energy change resulting from a change in the solute size is to be determined. In this case the only interaction potential that changes is the interaction of the solute with the water. Furthermore, if the mass of the solute is kept constant, the kinetic part of the Hamiltonian does not change during the mutation and it is only necessary to consider the configurational energy.

The configurational energy of the end points is given by U_1 at $\lambda = 1$ and U_0 at $\lambda = 0$. A series of intermediate points denoted by $\lambda = \lambda_j$ are then examined. The energy at $\lambda = \lambda_j$ is given by the following linear interpolation of the energies of the two end points:

$$U(\lambda) = (1-\lambda)U_0 + \lambda U_1. \tag{6}$$

We illustrate this in Fig. 1 using a simple example. The initial state is a Lennard-Jones neon atom in water and so the energy U_1 is given by the Lennard-Jones potential curve for the neon-oxygen interaction. The final energy U_0 is given by the Lennard-Jones potential curve for the argon-oxygen interaction. At any intermediate point $\lambda = \lambda_j$, the energy $U(\lambda)$ is a linear combination of the two Lennard-Jones potentials.

Rearranging Eq. (6) yields

$$U(\lambda) = U_0 + \lambda(U_1 - U_0), \tag{7}$$

and differentiating with respect to λ gives

$$\frac{\partial U(\lambda)}{\partial \lambda} = U_1 - U_0. \tag{8}$$

The change in free energy for the reaction is then given by

$$\Delta G = \int_0^1 \frac{\partial G(\lambda)}{\partial \lambda} d\lambda = \int_0^1 \left\langle \frac{\partial U(\lambda)}{\partial \lambda} \right\rangle_\lambda d\lambda. \tag{9}$$

The ensemble average is replaced by a time average and calculated in the simulation for each of the chosen values of λ. As can be seen from Eq. (8), this involves simulating at a particular point λ_j, calculating the energy of the initial and final states for this configuration, forming their difference, and averaging this quantity over the course of the simulation. The final value for the free energy is given by a separate numerical integration using, for example, Gauss-Legendre integration.

A similar process uses a nonlinear interpolation between the two end states, for example, taking

$$U(\lambda) = (1-\lambda^2)U_0 + \lambda^2 U_1. \tag{10}$$

This process is no more complicated than the linear case, although it should be noted that the parameter λ will now appear explicitly in the partial derivative. Any functional form for $U(\lambda)$ can be used as long as when $\lambda = 1$ the energy is U_1, and when $\lambda = 0$ the energy is U_0. Alternative pathways have advantages in some situations such as overcoming the singularity problem associated with the creation or annihilation of a particle.[3]

B. CF1 central force model of water

The CF1 central force model of water[51] was developed[52,53] from the revised central force model of water.[54] The model consists of three spherically symmetric potentials describing the OO, OH, and HH interactions in the water,

$$\begin{aligned} U_{\mathrm{HH}} &= \frac{36.1345}{r} + \frac{18}{1+e^{40(r-2.05C_2)}} \\ &\quad - 17e^{-7.621\,77(r-1.452\,51)^2} \\ U_{\mathrm{OH}} &= \frac{-72.269}{r} + \frac{6.234\,03}{r^{9.199\,12}} - \frac{10}{1+e^{40(r-1.05)}} \\ &\quad - \frac{4}{1+e^{5.493\,05(r-2.2)}} \\ U_{\mathrm{OO}} &= \frac{144.538}{r} + \frac{26\,758.2C_1}{r^{8.8591}} - 0.25e^{-4(r-3.4)^2}, \end{aligned} \tag{11}$$

where r is the distance between two atoms in Å and the energies have units of kcal mol^{-1}. The constants C_1 and C_2 can be varied to give the original CF potential of Stillinger and Rahman[54] ($C_1 = C_2 = 1$) or the modified CF1 potential[51] ($C_1 = 0.9$, $C_2 = 1/1.025$). The CF1 potentials are shown in Fig. 2.

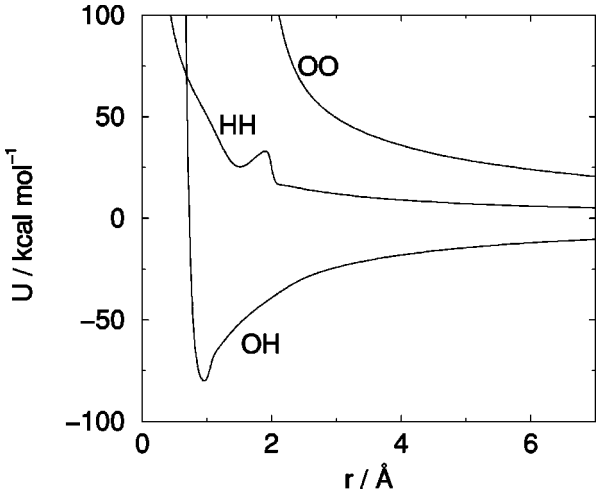

FIG. 2. The CF1 potential model of water.

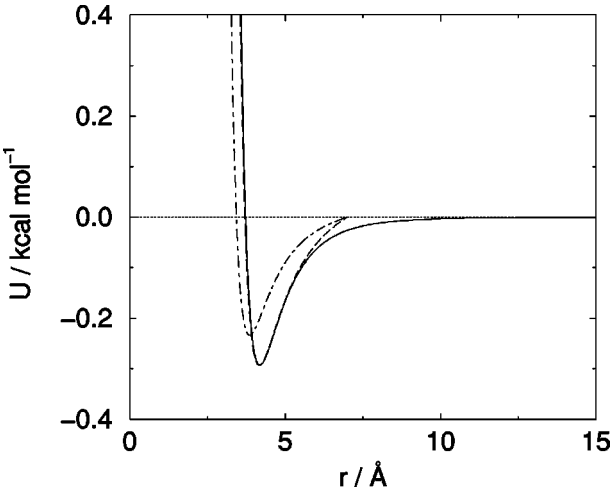

FIG. 3. Lennard-Jones based models for the interaction of methane with the oxygen atom in the water molecules. The solid line shows the true Lennard-Jones potential with its long ranged tail. The dot-dashed line shows the shifted-force potential. The dashed line shows the modified shifted-force potential.

The CF1 model is an atom-based model of water. The hydrogen and oxygen atoms are treated as individual atoms and both the intramolecular and intermolecular potentials are given by the potentials listed above. A partial charge of $q_H = 0.329\,83e$, where e is the proton charge, is assigned to each hydrogen atom. The oxygen atoms each carry a charge of $q_O = -2q_H$.

C. Modified shifted-force potentials

The solutes in this study are modeled by simple Lennard-Jones spheres. The Lennard-Jones potential of interaction of the solute molecule with the surrounding water is

$$U(r_{\mathrm{SO}}) = 4\epsilon_{\mathrm{SO}}\left(\left(\frac{\sigma}{r_{\mathrm{SO}}}\right)^{12} - \left(\frac{\sigma}{r_{\mathrm{SO}}}\right)^{6}\right), \tag{12}$$

where r_{SO} is the distance between the oxygen atom on the water molecule and the solute. There is no explicit interaction between the hydrogens of the water and the solute molecule. We use as our reference point in this study the Lennard-Jones parameters of methane used by Smith and Haymet,[21] which were developed by Jorgensen *et al.*[55] A plot of the Lennard-Jones potential for methane using these parameters is found in Fig. 3. In our simulations we truncated the potentials at 7 Å. As seen in Fig. 3, the Lennard-Jones potential (solid line) has a nonzero energy at this cut-off distance. The remaining tail must be accounted for in some way; otherwise the jump in energy will cause instabilities in the algorithm and result in erroneous values for any properties measured.

In this study, shifted-force potentials are used to treat this tail. In this method the tail is removed by shifting the potential and force curves so they both go smoothly to zero at the point of potential cut-off. This method is described by Haile[56] and has previously been used to generate a short-range version of the CF1 potentials.[57]

The force curves have been shifted first by adding (or subtracting) a small quantity equal to the magnitude of the force at the cut-off point. In this way the force becomes smoothly zero at the cut-off point. The shifted force $F_s(r)$ is given by

$$F_s(r) = \begin{cases} -dU/dr + \Delta F & r \leqslant r_c \\ 0 & r > r_c \end{cases}, \tag{13}$$

where r_c is the desired cut-off distance for the potential U and ΔF is the magnitude of the shift given by

$$\Delta F = -F(r_c) = \left(\frac{dU}{dr}\right)_{r_c}. \tag{14}$$

The shifted force can then be integrated to generate a new potential. This potential function will be the original potential plus an extra linear term arising from the integration of the constant term added to the force. This new potential can then be shifted to achieve a potential curve that goes smoothly to zero at the cut-off point, in the same manner as was done for the force. (The addition of the constant to the potential curve has no effect on the force curve because the constant is removed when differentiation takes place.) The new potential is then given by

$$U_s(r) = \begin{cases} U(r) - U(r_c) - [r - r_c]\left(\dfrac{dU}{dr}\right)_{r_c} & r \leqslant r_c \\ 0 & r > r_c \end{cases}. \tag{15}$$

Figure 3 shows the shifted-force potential for the Lennard-Jones model of the interaction of water and solute (dot-dashed line). The new shifted-force potential can be seen to go smoothly to zero at the cut-off point of 7 Å. A comparison of the shifted-force potential and the true Lennard-Jones potential shows that the shifting process changes the depth of the potential well. It is important to note that for both these curves the value of ϵ is the same but the well depth is *different*. Another effect of the shifting technique is that the amount by which the depth of the potential well in the shifted-force curve differs from that of the original curve varies according to the value of σ. The smaller the value of σ, the quicker the Lennard-Jones curve goes to zero. Hence a potential curve with a smaller value of σ will require less

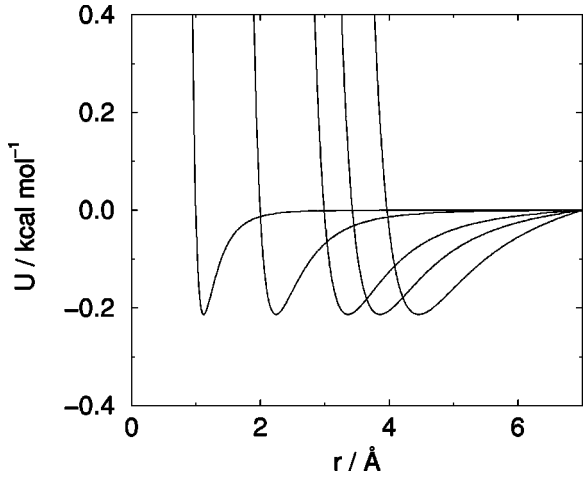

FIG. 4. A set of modified shifted-force potentials used in the simulation of nonpolar solutes in water. Each potential represents a solute of differing size at a constant well depth equivalent to the depth of the Lennard-Jones methane potential curve. From left to right the value of σ is 1, 2, 3, 3.4475 and 4 Å.

shifting for a fixed cut-off length. The result of this is that if we keep ϵ constant and vary σ, the depth of the well will change over the range of σ, becoming shallower as σ becomes larger.

In this study we are interested in the effect of changing the solute size while keeping the well depth constant. Thus it becomes necessary to adjust the value of ϵ to keep the actual well depth constant when using the shifted-force potentials. A simple numerical program can be used to calculate the required value of ϵ. Figure 3 shows the modified shifted-force potential for the interaction of a methane molecule with a water molecule. As can be seen by modifying the value of ϵ, the shifted-force curve is modified so the well depth is coincident with that of the original Lennard-Jones potential. Figure 4 shows the potential curves for a series of solutes of different sizes. The well depth is now constant across the entire range of solute sizes due to the adjustment of ϵ. Throughout this paper σ refers to the solute size (from the solute-water interaction potential) and ϵ refers to the actual well depth, that is, the depth of the true Lennard-Jones potential.

IV. MOLECULAR DYNAMICS SIMULATIONS

All molecular dynamics simulations have been performed using a locally developed program called CFW1. Water has been modeled by the CF1 central force model of water.[51] A simulation box of 108 water molecules (composed of 108 oxygen atoms and 216 hydrogen atoms) was used. Preliminary simulations performed for 216 water molecules, as a partial check for finite-size effects, yielded free energy differences which agree within the stated error estimates. The nonpolar solute was modeled as a spherically symmetric Lennard-Jones sphere. The interaction of the solute with the oxygen atom of the water molecule is assumed to be pairwise additive, and given by Eq. (12), shifted and modified as described above. As a test, the interaction of the solute molecule with the hydrogen atoms of the water molecule was initially modeled by a purely repulsive, very short-range, soft-sphere potential

$$U(r_{\mathrm{SH}}) = 4\epsilon_{\mathrm{SH}}\left(\frac{\sigma}{r_{\mathrm{SH}}}\right)^{12}. \tag{16}$$

Preliminary simulations have been performed to check the effect of this repulsive solute-hydrogen potential on the energy of the system. As intended, we found the solute-hydrogen potential energy contributed less than 1 part in 10^8 of the total energy. This is due to the radius of the oxygen atom being large enough to ''encompass'' the hydrogen atoms of the water, effectively screening any interaction they might have with the solute atoms. Subsequently, the solute-hydrogen potential function was set to zero.

The equations of motion were integrated using a five-value first-order Gear predictor-corrector algorithm. The time step varied among simulations from a minimum of 0.05 to a maximum of 0.2 fs. All simulations were performed in the NPT ensemble with a temperature of 298 K and pressure of 1 atm. The temperature and pressure have been constrained using a Nosé-Hoover thermostat and barostat[58] with coupling constants of 0.006 and 0.5 ps, respectively. The Coulombic terms in the potential energies have been treated using the Ewald summation technique.[59] The minimum image convention has been used for all the short-ranged terms. Standard cubic periodic boundary conditions have been used.

Statistical uncertainties throughout this work have been calculated using the block averaging technique. The final average was decomposed into a series of sub-averages. The uncertainty in the mean is calculated from the resulting distribution. All uncertainties are reported throughout as $\pm 2\sigma$ (where σ is one standard deviation), that is, approximately 95% confidence limits.

V. RESULTS AND DISCUSSION

A. Systematic exploration of the free energy surface

A series of simulations was performed to examine the change in free energy with solute size and potential well depth. A system comprising one methane molecule and 107 water molecules was chosen as the reference state. This system was thoroughly equilibrated prior to the exploration of the free energy surface. Each state point on the free energy surface was defined by its unique values of σ and ϵ. The relative free energy of each state point was given by the difference in free energy between the reference state and the desired state point, calculated using linear thermodynamic integration. The absolute free energy of the reference state was taken to be 2.0 kcal mol^{-1} exactly. The justification for this choice is given in the Appendix. This value was added to the difference to give the absolute free energy for each state point. The partial derivative of the relative free energy was calculated at eight intermediate points, determined by the eighth-order Gauss-Legendre integration methodology. The simulations were performed in the NPT ensemble with a time step of 0.2 fs. Each intermediate point was equilibrated

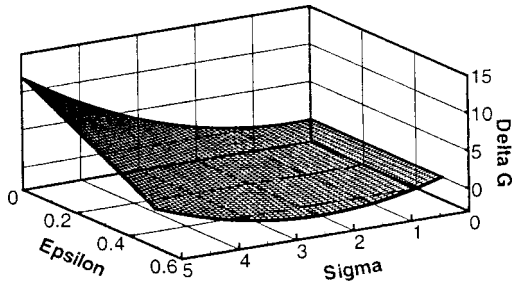

FIG. 5. A three-dimensional plot showing the free energy surface as a function of the size of the solute and the depth of the solute-water potential well. σ has units of Å, and ϵ and ΔG have units of kcal mol^{-1}.

for 4 ps prior to the accumulation of the ensemble averages over another 4 ps. Hence the total simulation time for each state point on the surface was 64 ps.

Alternate methods for generating the surface have also been considered. For example, the free energy of each state point could be calculated relative to a nearby state point rather than having all free energies calculated relative to *one* reference point. Thus, in changing the solute size from 4 to 1 Å in 1 Å steps, the first calculation could determine the relative free energy between 3 and 4 Å, the second between 2 and 3 Å, and the third between 1 and 2 Å. Using this method, the difference between the two state points, for which a free energy difference is being determined, is minimized, making each individual calculation more accurate. In contrast, the method we have chosen uses the same number of time steps to calculate the free energy of each state point. Thus the free energy of a state point further from the reference point is likely to have a higher error associated with it because the difference between the state point and the reference point is larger. However, by using a single reference point, the surface can be generated more easily by adding the absolute free energy of the reference point to the relative free energy of each state point. Using the alternate method, many additions along the chain of ''reference states'' need to be performed. The use of a single reference state also allows us to easily modify the free energy surface given a more accurate calculation of the absolute free energy of the reference point. The error in the free energies calculated using the alternative method also tends to be larger than the error in those calculated by our chosen method. When moving along the chain of reference states in the alternative method, the error in each calculation accumulates using standard rules of error propagation. A preliminary series of calculations using this technique showed that the error in the free energy of each state point, given the many accumulations, tends to be larger than the error associated with moving straight from a single reference state. Given these advantages we chose the single reference state method as the most effective.

Figure 5 shows a three-dimensional plot of the free energy surface. Sixteen states have been chosen to give a surface covering a range of solute sizes from 1 to 4 Å and potential well depths from 0.1 to 0.4 kcal mol^{-1} in steps of 1 Å and 0.1 kcal mol^{-1}, respectively. Another four states have been chosen by holding the solute size constant at 3.4475 Å (the value used for the reference state) and changing the well depth over the same range as above, and another four by, similarly, keeping the well depth constant at 0.2134 kcal mol^{-1} and changing the solute size. The surface shown in Fig. 5 is the surface of best fit to the free energies of the state points. Initially all linear and quadratic functions in the two parameters were included to determine the curve of best fit. We then noted that as the solute size goes to zero the free energy must go to zero also. Thus a further restriction on the surface was that the free energy be zero when $\sigma=0$ for all values of ϵ. For clarity, Fig. 5 does not show the error bars associated with each point.

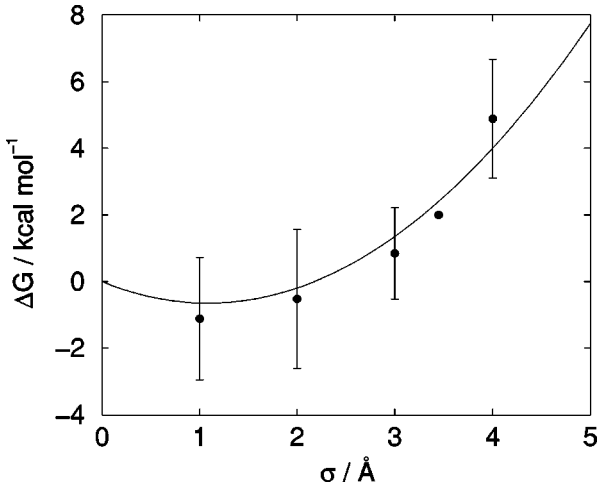

FIG. 6. A slice through the free energy surface of Fig. 5 showing the variation of free energy with solute size at $\epsilon=0.2134$ kcal mol^{-1}.

B. Change in free energy with solute size

Figure 6 shows a slice through the 3D surface of Fig. 5 for the state points having $\epsilon=0.2134$ kcal mol^{-1}, the well depth of the reference state. Also shown are the error bars for each point on the surface. Similar plots for the other values of ϵ are in Fig. 7. The surface passes smoothly through the

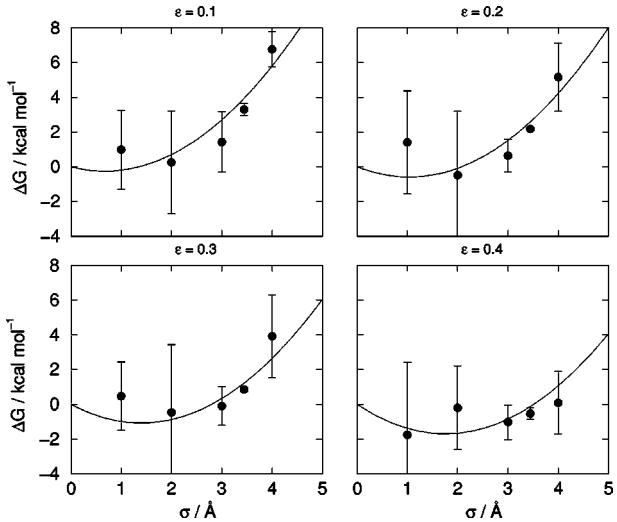

FIG. 7. Slices through the free energy surface of Fig. 5 of constant potential well depth showing the variation of free energy with solute size. The values of ϵ in kcal mol^{-1} are labeled.

error bars of most points. The error bars are within acceptable limits even though reasonably large. The size of the error bars can be reduced by increasing the length of the simulation used to calculate the free energy of each state point, giving better sampling of the configuration space and hence a better value for the free energy. It is also possible to improve the results by using more intermediate points in the determination of the relative free energy of each state point, i.e., by using a higher order Gauss-Legendre algorithm. However, the results (not shown) of a test case involving the calculation of the absolute solvation free energy of methane using 12 intermediate points showed no significant improvement over the results from the previous method using 8 intermediate points.

The curves are remarkably similar in appearance over the range of well depths they represent. As the size of the solute increases, the free energy of insertion also generally increases, although the curve of best fit appears to indicate a slight minimum in the free energy of solvation for smaller solutes. This minimum is likely to be an artifact of the curve fitting program and the larger error in the free energy for the small solutes. An alternative explanation is that, for small solutes with a deep potential well, the favorable enthalpic contribution to the free energy of solvation could overcome the unfavorable entropic contribution. This is supported by the results shown in Fig. 7, where the minimum in the free energy curves becomes increasingly pronounced as the depth of the potential well increases. However, previous simulations suggest that even solutes of negligible size have a highly unfavorable entropy of solvation.[38] Further, more precise simulations are needed to resolve this point.

The insertion of a nonpolar solute is an unfavorable process. There are two explanations for this. The first explanation assumes that, in general, the solute forces the water molecules to become more ordered as they structure themselves to accommodate the solute, thus causing a large unfavorable entropic effect. The second dissects the process of solvation into two components, the formation of a cavity in the water to accommodate the solute and the interaction of the solute with the water molecules. In this model the creation of a cavity restricts the motion of the solvent particles. A large number of configurations originally available to the solvent particles become unavailable. This causes an unfavorable entropic effect that is particularly large in water due to the small molecular volume of the water molecule. The latter is the generally accepted model.[38] As the solute becomes larger, more water molecules are affected by its presence. The larger cavity required to accommodate the solute makes even more solvent configurations unavailable, thus increasing the entropy. (In the alternate view the amount of restructuring and ordering of the water molecules to accommodate the solute increases, thus increasing the entropy.) Perkyns and Pettitt[40] showed that the major contribution to the free energy is the entropy. Furthermore, Lazaridis and Paulaitis[22] showed, through their study of the entropy of solvation, that the solute size is the main parameter contributing to the entropy of solvation. This agrees with our results. The effect of changing the solute size on the free energy of solvation is much more marked than the effect of changing the depth of the potential well. The variation of the free energy with solute size can be modeled adequately by a quadratic function, whereas the variation with potential well depth is modeled adequately by a linear function. Thus larger solutes are increasingly difficult to solvate, as shown by the increasing free energy of solvation.

C. Free energy of solvation for small solutes

While the larger solute sizes clearly exhibit the trends discussed above, difficulties arise as the solute size approaches zero. As can be seen in Figs. 6 and 7, the free energy of solvation for small solute sizes has a higher error associated with it. Furthermore, the absolute value of the free energy at these points does not clearly follow the trend experienced in the points at larger solute sizes. This difficulty is also evident from the plots of the variation of free energy with potential well depth shown in Fig. 9 and discussed in greater detail below. The results for $\sigma=1$ show a much larger scatter in the points, larger error bars, and generally a worse agreement with the free energy surface of best fit compared to the other values of σ. Reference to Fig. 4 shows that keeping the well depth constant using the modified shifted-force potentials results in narrow potentials for small solutes. The narrowness of the potential well gives rise to the problems described above. The steep walls of the potential well mean that a small change in the position of the solute with respect to nearby water molecules results in a large change in the potential energy. Thus in a molecular dynamics simulation, a small time step is required to correctly resolve this potential well. The time step used in our simulations (0.2 fs) was unable to resolve this well adequately, resulting in the solute spending an abnormally large amount of the simulation time at high energy regions of the potential curve. In an effort to solve this problem we systematically decreased the time step to 0.05 fs. There was no significant improvement in the final value of the free energy and no significant reduction in the size of the error associated with this value. Time steps smaller than 0.05 fs have not been attempted due to the prohibitively long amounts of simulation time required to perform simulations of the same total time as the other simulations in the series.

We also attempted to resolve the narrow well by altering the method used to equilibrate the system at each intermediate point. As mentioned previously, the relative free energy of each state point was calculated using eight intermediate stages. Each stage was equilibrated for 4 ps prior to accumulating the averages over the next 4 ps. Thus, after accumulating the averages at one stage, the system undergoes a ''jump'' to the next stage, where the equilibration and averaging is repeated. Another explanation for the poor sampling of systems involving small solutes is that on ''jumping'' to the very narrow wells the system enters a highly nonequilibrium state and never fully escapes this state. In order to check this possibility, a process of adiabatic equilibration was utilized. In this method the sudden ''jump'' followed by 4 ps of equilibration was replaced by 2 ps where the system gradually moves from the previous stage to the new stage, followed by a further 2 ps of equilibration at the new stage. It was hoped that using this method, the solute would ease

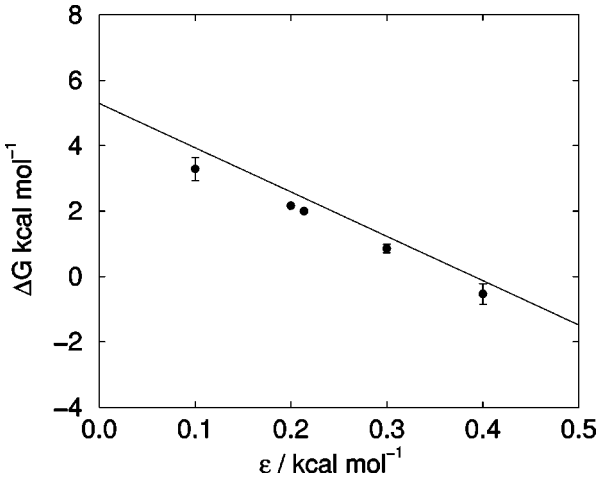

FIG. 8. A slice (shown by the solid line) through the free energy surface of Fig. 5 showing the variation of free energy with potential well depth at $\sigma = 3.4475$ Å.

into and remain in the narrow potential wells. We tested this method on the calculation of the free energy at the state point with parameters $\sigma = 1$ Å and $\epsilon = 0.2134$ kcal mol^{-1}. No improvement in the result was obtained; both the result and the error were worse than those obtained with the previous method. Thus it appears the difficulty associated with the narrow potential wells will only be solved by lengthy calculations using a very small time step.

D. Change in free energy with potential well depth

In a similar way it is possible to take slices through the free energy surface in Fig. 5 at values of constant solute size. Figure 8 shows a slice through the 3D surface for the state points at $\sigma = 3.4475$ Å, the solute size of the reference state. Similar plots for the other values of σ are in Fig. 9. Once again the best fit surface to the various state points goes smoothly through the error bars of most points on the various curves.

The change in free energy with a change in the depth of the potential well is much smaller than the corresponding change due to a change in the solute size. This shows that the strength of the interaction between the water molecules and the solute has much less effect on the free energy of solvation than the size of the solute. As mentioned before, this agrees with previous results.[22]

It is interesting to note that the error in the free energy calculated from simulations changing purely the depth of the potential well, is much less than the error in the free energy calculated in simulations that also involve a change in the solute size. Once again we draw attention to the fact that the free energy of each point on the surface is calculated relative to one reference state. This means the free energy of most points on the surface is obtained by a series of intermediate simulations changing the solute size and well depth simultaneously. At first this seems to contradict our claim that we have plotted the change in free energy with solute size at constant well depth. However, the key point is that for all state points on each curve in Fig. 7 the depth of the potential well is exactly the same. This is in contrast to similar results in the literature[11,12,22] where the calculated entropies and free energies for each solute size have a different well depth associated with them. There is one curve, though, where not only are all the points at constant solute size but all the simulations involve only changing the well depth. This curve is found in Fig. 8 for $\sigma = 3.4475$ Å. It is evident that when the simulations involve only a change in well depth the configuration space is more fully sampled and the resulting free energies are more precise.

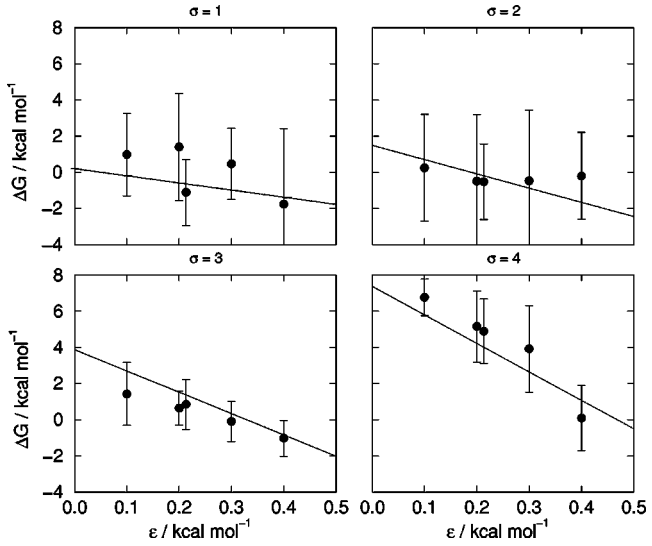

FIG. 9. Slices through the free energy surface of Fig. 5 of constant solute size showing the variation of free energy with potential well depth. The values of σ in Å are labeled.

E. Noble gas series

In order to compare with previous work, a separate series of simulations was performed to study the solvation of the noble gases under similar conditions to those used in the generation of the free energy surface. The system comprising one methane solvated in 107 water molecules was chosen as a reference point and six other states chosen to correspond to the six noble gases. The relative free energy of each state point was calculated relative to the reference state using linear thermodynamic integration with eight intermediate steps at stages determined by the Gauss-Legendre integration. Each intermediate stage was equilibrated for 4 ps followed by accumulation of the averages over another 4 ps. The time step used was 0.2 fs and the simulations have been performed in the NPT ensemble. In this series a change in size of the solute is accompanied by a change in the potential well depth. The potentials used to model this change have been taken from two papers. Guillot *et al.*[11] examined the free energies of solvation of the noble gases from neon to xenon (and also methane). Straatsma *et al.*[39] also studied the solvation of the noble gases and their results have been reformulated by Guillot *et al.* for comparison with their own work. Lazaridis and Paulaitis[22] performed similar calculations studying the entropy of solvation of gases in the wider series from helium to radon. We chose the parameters used

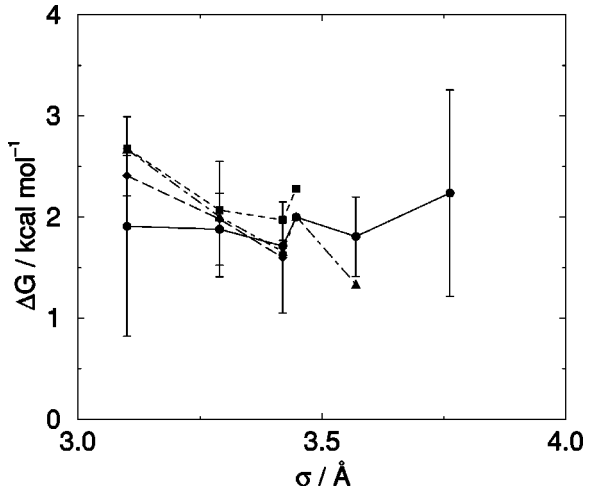

FIG. 10. Variation of free energy with solute size for the series of noble gases from neon to radon. The solid line is the result from this work, the dashed line is from Guillot *et al.* (Ref. 11), the long dashed line from Straatsma *et al.* (Ref. 39) as reported in the paper by Guillot *et al.*, and the dot-dashed line is from experimental results compiled by Ben-Naim and Marcus (Ref. 60). No error bars were reported in the latter two papers.

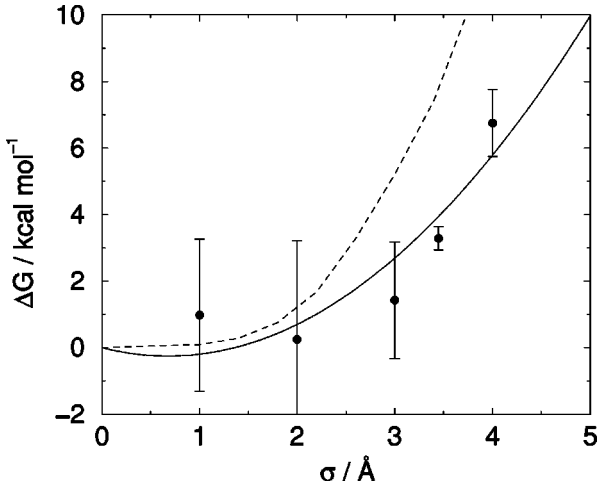

FIG. 11. A comparison of the variation of free energy with solute size as calculated from simulation (solid line) and information theory approximation for solvation of hard spheres (dashed line). The simulation results use the parameter $\epsilon = 0.1$ kcal mol^{-1}.

by Guillot *et al.* because their methane parameters were almost identical to those used in this work. The parameters of Lazaridis and Paulaitis have been used for our helium and radon solutes. The Lennard-Jones parameter, ϵ, taken from the papers, was modified so the depth of the shifted-force potential curve is the same as the original Lennard-Jones curve.

The results of this series are shown in Fig. 10, where the variation of free energy is given as a function of solute size. It is important to remember that each point on this curve has a different value of ϵ associated with it. The figure also plots the results of Guillot *et al.*,[11] Straatsma *et al.*,[39] and experiment.[60] Our results show the free energy of solvation for the Lennard-Jones models of neon through to radon. (The solvation free energy of the classical Lennard-Jones model of helium is not shown because the value we calculated, 0.103 ± 2.101 kcal mol^{-1}, had a very large error associated with it. Given this error and the lack of previous measurements of this quantity for comparison, we are unconvinced of the reliability of this point.)

The trend for the free energy to increase with increasing solute size is not as evident in this series compared to our previous simulations. Although there is a general trend of increasing free energy, the individual points show a large amount of scatter. This is due to the effect of the different depths of the potential well associated with each point. The effect of the depth of the potential well is significant enough to affect the trends observed in the free energy as the solute size increases. The large error in the helium state point makes it difficult to determine whether the free energy of solvation of helium is really that low or whether it should more correctly lie around the reasonably similar values of the other gases in the series.

Our results agree very well with the results of Guillot *et al.*,[11] Straatsma *et al.*,[39] and experimental measurement.[60] The general trends are the same, i.e., a slight decrease from neon to krypton followed by a sharp increase to methane and then a decrease to xenon. This confirms that the CF1 model of water can be used to calculate free energy differences comparable to experimental results and results from simulations with other models of water.

Finally, the solute size for helium, one of the smallest possible real nonpolar solutes, is approximated by $\sigma = 2.8575$ Å. Thus the difficulties of calculating the free energy of solvation for solutes of smaller sizes becomes a somewhat academic problem. It is nevertheless interesting and important to our understanding of hydrophobic hydration to study the trends in solvation free energy for these very small (theoretical) solute sizes.

F. Comparison with theoretical approximations

As a further check on the accuracy of our results, we compared them with theoretical results obtained using the information entropy maximization approach of Hummer *et al.*[42–44] Details of the method can be found in their papers; a brief description is given here for completeness. Their papers, as well as others,[61,62] describe applications of the method to a range of solvation phenomena. The method provides a way of determining the free energy of solvation of hard spheres in a solvent (e.g., water) from information derived from the simulation of pure solvent. We calculated the density and oxygen-oxygen pair correlation function from a simulation of a box of 108 water molecules. The density and pair correlation function have been used to determine the first and second moments of the fluctuation of spontaneous cavities of a size large enough to contain the solute of interest. The probability distribution, $\{p_n\}$, was calculated from these moments using the information entropy maximization technique. (p_i is the probability of finding a cavity in pure water, large enough to contain the solute, containing i water molecules.) The free energy of solvation was determined from p_0. This was repeated for a number of solutes of various sizes. (The simulation of pure water only needs to be done once, but the entropy maximization needs to be done

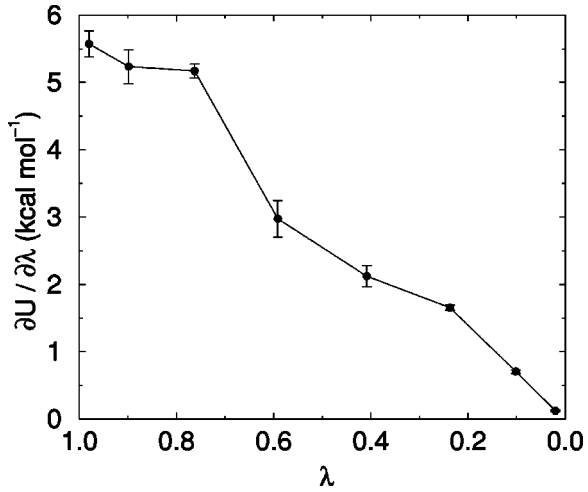

FIG. 12. Variation of the partial derivative of the energy with respect to the reaction coordinate plotted as a function of the reaction coordinate. Integration of this curve allows the calculation of the absolute free energy of solvation for methane in the CF1 model of water.

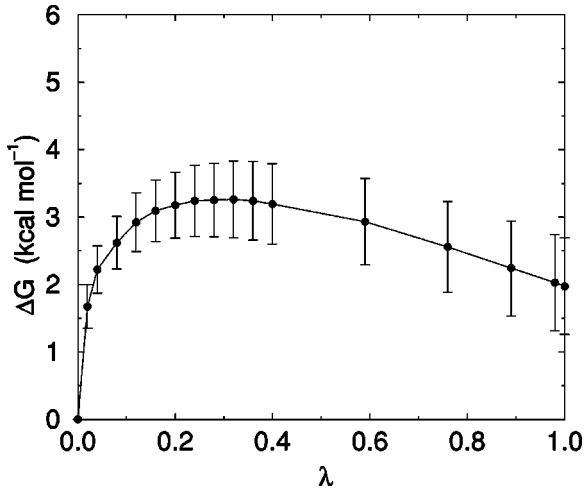

FIG. 13. The cumulative free energy of solvation of methane, in the Kofke method. Each point on the curve represents a stage in the insertion of the methane solute into the water. The total free energy and its associated error up to that stage are shown.

for each solute size.) The results are plotted in Fig. 11, together with the results from the constant well depth curve of $\epsilon = 0.1$ kcal mol^{-1}. The curve with the shallowest potential well has been used because it most closely approximates the hard sphere potential used in the information theory method. The results are again interesting. Once again the same trend in the variation of free energy with solute size is evident; the free energy increases nonlinearly as the solute size increases. The free energies calculated using information theory are systematically higher than the results from our simulations. This is to be expected because the information theory results are for hard sphere insertions.[63] A more detailed comparison with solutes of variationally chosen hard sphere diameter is presented elsewhere.[62]

VI. CONCLUSIONS

We have shown the thermodynamic integration technique can be used to calculate the free energy of solvation of nonpolar solutes in water. The CF1 model of water was used. The absolute free energy of solvation of methane in CF1 water compared very well with similar calculations in alternative models of water and experiment. This shows the CF1 model of water is adequate for use in free energy calculations.

The free energy of solvation of nonpolar solutes has been systematically examined by independently changing the size of the solute and the depth of the solute-water interaction potential. The solute size was found to be the primary parameter affecting the free energy; however, the depth of the potential well did have a significant effect on the resulting free energy. The change in free energy with solute size could be adequately modeled by a quadratic function whereas the change with potential well depth was approximately linear. Thus simulations of the noble gas series and other homologous series, where both the size of the solute and the strength of its interaction with the water change, cannot adequately examine the trends in the variation of the free energy with either parameter. By exploring the free energy surface in a systematic way, we have shown that the free energy increases rapidly with increasing solute size and also decreases slightly with increasing depth in the solute-water potential. Difficulties in measuring the free energy of solvation for narrow potential wells have been noted and further examination of this difficulty led to the conclusion that very small time steps are needed to resolve these problems.

A series of studies on the solvation of the noble gases shows that our results again agree well with previous work, confirming the viability of the CF1 potentials for use in free energy calculations. Finally, we compared our results to the solvation free energy of hard spheres in CF1 water calculated with an information theory technique. Our results compare well, being slightly lower than the hard sphere results, as expected by the differences in the model used for the solute-water interaction.

ACKNOWLEDGMENTS

J.W.A. gratefully acknowledges support from a DEETYA APA scholarship. In Australia, this research was supported by the Australian Research Council (ARC) (Grant No. A29530010), SydCom, the USyd/UTS Distributed Processing Facility funded by an ARC infrastructure grant, and the NSW Center for Parallel Computing.

APPENDIX A: THE FREE ENERGY OF SOLVATION OF METHANE

Simulations have been performed in order to measure the absolute solvation free energy of methane in water. A methane solute was inserted into a box of water and this system was equilibrated thoroughly. The absolute free energy was calculated by the technique of thermodynamic integration as described in the Sec. III A. The initial state was defined as the equilibrated methane and water system where the methane-water interaction was given by the shifted-force Lennard-Jones potential. In the final state the methane mol-

TABLE I. Various literature results for the free energy of solvation of methane in water. Note that some of the papers listed in the table give more than one value for the free energy. This is usually due to different methods of calculation or simulation conditions.

Water potential	Methane potential	Free energy
Experiment	Experiment	1.932[a]
TIP4P	LJ	2.5 ± 0.4[b]
TIP3P	AMBER[c]	2.12 ± 0.90[d]
TIP3P	AMBER	2.09 ± 0.09[e]
		2.02 ± 0.31
		2.81 ± 0.03
		2.44 ± 0.49
TIP3P	AMBER	2.36 ± 0.07[f]
		3.52 ± 0.21
		3.67 ± 0.15
TIP3P	AMBER	0.76 ± 0.36 to 1.76 ± 0.04[g]
TIP3P	LJ	2.11 ± 0.14[h]
		1.19 ± 0.16
SPC	LJ	2.28[i]
TIP3P	AMBER	1.91[j]
		2.71

[a]Reference 60.
[b]Reference 6.
[c]Reference 65.
[d]Reference 4.
[e]Reference 5.
[f]Reference 8.
[g]Reference 64.
[h]Reference 14.
[i]Reference 11.
[j]Reference 66.

ecule no longer interacts with the water. The methane was removed by gradually turning off the potential of interaction between the methane and the water molecules.

Figure 12 shows a plot of $\partial U/\partial\lambda$ with λ. The curve was obtained with a second order thermodynamic integration algorithm. The partial derivative decreases relatively smoothly and almost linearly as the system moves along the reaction coordinate from the initial state to the final state. This is an indication the system sampled configuration space accurately in the vicinity of the singularity where the solute-water interaction potential becomes zero. Integrating this curve gives a value of 2.94 ± 0.14 kcal mol^{-1} for the absolute free energy of solvation of methane in water.

We also measured the absolute free energy of solvation of methane using the staged insertion technique of Kofke and Cummings.[48] A box of 107 water molecules was equilibrated thoroughly. The methane solute was then inserted in a series of 16 stages. The free energy of solvation of methane was determined by taking the sum of the changes in the free energy for each stage of the insertion process. Figure 13 shows the cumulative free energy over the course of the insertion process as defined by the reaction coordinate λ. Using this method the total free energy was found to be 1.973 ± 0.716 kcal mol^{-1}.

Both our results compare well with previous simulation results and experimental results as shown in Table I. Our results are well within the range of results measured by other researchers using various models for water and methane. This confirms that the CF1 model of water accurately reproduces the free energy of solvation of methane. Based on our calculations we chose a reference point for our exploration of the free energy surface of 2.0 kcal mol^{-1} exactly. This is a convenient value in good agreement with our calculated values, experimental measurements, and other estimations of the quantity from molecular simulations.

[1] B. J. Alder and T. E. Wainwright, J. Chem. Phys. **31**, 459 (1959).
[2] N. Metropolis, A. W. Rosenbluth, M. N. Rosenbluth, A. H. Teller, and E. Teller, J. Chem. Phys. **21**, 1087 (1953).
[3] M. Mezei and D. L. Beveridge, Ann. (N.Y.) Acad. Sci. **482**, 1 (1986).
[4] P. A. Bash, U. C. Singh, R. Langridge, and P. A. Kollman, Science **236**, 564 (1987).
[5] D. A. Pearlman and P. A. Kollman, J. Chem. Phys. **90**, 2460 (1989).
[6] W. L. Jorgensen, J. F. Blake, and J. K. Buckner, Chem. Phys. **129**, 193 (1989).
[7] D. L. Beveridge and F. M. DiCapua, Annu. Rev. Biophys. Biophys. Chem. **18**, 431 (1989).
[8] D. A. Pearlman and P. A. Kollman, J. Chem. Phys. **94**, 4532 (1991).
[9] T. P. Straatsma and H. J. C. Berendsen, J. Chem. Phys. **89**, 5876 (1988).
[10] J. Quintana and A. D. J. Haymet, Chem. Phys. Lett. **189**, 273 (1992).
[11] B. Guillot, Y. Guissani, and S. Bratos, J. Chem. Phys. **95**, 3643 (1991).
[12] B. Guillot, Y. Guissanni, and S. Bratos, Russ. J. Phys. Chem. **67**, 30 (1993).
[13] T. Z. M. Denti, T. C. Beutler, W. F. van Gunsteren, and F. Deiderich, J. Phys. Chem. **100**, 4256 (1996).
[14] C.-L. Lin and R. H. Wood, J. Phys. Chem. **100**, 16,399 (1996).
[15] R. M. Lynden-Bell and J. C. Rasaiah, J. Chem. Phys. **107**, 1981 (1997).
[16] V. Helms and R. C. Wade, J. Comput. Chem. **18**, 449 (1997).
[17] S. Okazaki, K. Nakanishi, H. Touhara, N. Watanabe, and Y. Adachi, J. Chem. Phys. **74**, 5863 (1982).
[18] S. Okazaki, H. Touhara, K. Nakanishi, and N. Watanabe, Bull. Chem. Soc. Jpn. **55**, 2827 (1982).
[19] W. C. Swope and H. C. Andersen, J. Phys. Chem. **88**, 6548 (1984).
[20] D. E. Smith, L. Zhang, and A. D. J. Haymet, J. Am. Chem. Soc. **114**, 5875 (1992).
[21] D. E. Smith and A. D. J. Haymet, J. Chem. Phys. **98**, 6445 (1993).
[22] T. Lazaridis and M. E. Paulaitis, J. Phys. Chem. **98**, 635 (1994).
[23] S. R. Durell and A. Wallqvist, Biophys. J. **71**, 1695 (1996).
[24] S. J. Gill, S. F. Dec, G. Olosson, and I. Wadsö, J. Phys. Chem. **89**, 3758 (1985).
[25] K. A. T. Silverstein, A. D. J. Haymet, and K. A. Dill, Fluid Phase Equilib. (in press).
[26] K. A. T. Silverstein, A. D. J. Haymet, and K. A. Dill, J. Am. Chem. Soc. **120**, 3166 (1998).
[27] A. D. J. Haymet, K. A. T. Silverstein, and K. A. Dill, Faraday Discuss. **103**, 117 (1996).
[28] A. D. J. Haymet, K. A. T. Silverstein, and K. A. Dill, in *International Symposium on Molecular Thermodynamics and Molecular Simulation* (Hosei University, Tokyo, Japan, 1997), pp. 143–152.
[29] K. A. T. Silverstein, A. D. J. Haymet, and K. A. Dill, J. Am. Chem. Soc. (submitted).
[30] K. A. T. Silverstein, K. A. Dill, and A. D. J. Haymet, J. Phys. Chem. (in preparation).
[31] R. M. Levy and E. Gallicchio, Ann. Rev. Phys. Chem. (in press).
[32] A. Ben-Naim, *Hydrophobic Interactions* (Plenum, New York, 1980).
[33] K. A. Dill, Biochemistry **29**, 7133 (1990).
[34] D. F. Evans and B. W. Ninham, J. Phys. Chem. **90**, 226 (1986).
[35] C. Tanford, *The Hydrophobic Effect: Formation of Micelles and Biological Membranes* (Wiley, New York, 1973).
[36] O. K. Førrisdahl, B. Kvamme, and A. D. J. Haymet, Mol. Phys. **89**, 819 (1996).
[37] H. Wang and A. Ben-Naim, J. Med. Chem. **39**, 1531 (1996).
[38] W. Blokzijl and J. B. F. N. Engberts, Angew. Chem. Int. Ed. Engl. **32**, 1545 (1993).
[39] T. P. Straatsma, H. J. C. Berendsen, and J. P. M. Postma, J. Chem. Phys. **85**, 6720 (1986).
[40] J. Perkyns and B. M. Pettitt, J. Phys. Chem. **100**, 1323 (1996).
[41] G. Hummer, L. R. Pratt, and A. E. Garcia, J. Phys. Chem. **100**, 1206 (1996).
[42] G. Hummer, S. Garde, A. E. García, A. Pohorille, and L. R. Pratt, Proc. Natl. Acad. Sci. USA **93**, 8951 (1996).
[43] B. J. Berne, Proc. Natl. Acad. Sci. USA **93**, 8800 (1996).
[44] S. Garde, G. Hummer, A. E. Garcia, L. R. Pratt, and M. E. Paulaitis, Phys. Rev. E **53**, R4310 (1996).
[45] W. L. Jorgensen, J. Chandrasekhar, J. D. Madura, R. W. Impey, and M. L. Klein, J. Chem. Phys. **79**, 926 (1983).

[46] W. L. Jorgensen and J. D. Madura, Mol. Phys. **56**, 1381 (1985).
[47] D. A. McQuarrie, *Statistical Mechanics* (Harper and Row, New York, 1975).
[48] D. A. Kofke and P. T. Cummings, Mol. Phys. **92**, 973 (1997).
[49] T. P. Straatsma and J. A. McCammon, J. Chem. Phys. **95**, 1175 (1991).
[50] M. Abramowitz and I. A. Stegun, *Handbook of Mathematical Functions with Formula, Graphs, and Mathematical Tables*, 7th ed., National Bureau of Standards Applied Mathematics Series 55 (National Bureau of Standards, Washington D.C., 1968).
[51] D.-M. Duh, D. N. Perera, and A. D. J. Haymet, J. Chem. Phys. **102**, 3736 (1995).
[52] D. E. Smith and A. D. J. Haymet, J. Chem. Phys. **11**, 8450 (1992).
[53] A. Nyberg and A. D. J. Haymet, ACS Symp. Ser. **568**, 110 (1994).
[54] F. H. Stillinger and A. Rahman, J. Chem. Phys. **68**, 666 (1978).
[55] W. L. Jorgensen, J. D. Madura, and C. J. Swenson, J. Am. Chem. Soc. **106**, 6638 (1984).
[56] J. M. Haile, *Molecular Dynamics Simulation: Elementary Methods* (Wiley, New York, 1992).
[57] J. W. Arthur and A. D. J. Haymet, Fluid Phase Equilib. (in press).
[58] S. Melchionna, G. Ciccotti, and B. L. Holian, Mol. Phys. **78**, 533 (1993).
[59] M. P. Allen and D. J. Tildesley, *Computer Simulation of Liquids* (Oxford University Press, New York, 1989).
[60] A. Ben-Naim and Y. Marcus, J. Chem. Phys. **81**, 2016 (1984).
[61] G. E. Crooks and D. Chandler, Phys. Rev. E **56**, 4217 (1997).
[62] J. W. Arthur and A. D. J. Haymet (in preparation).
[63] S. Garde, G. Hummer, A. E. García, M. E. Paulaitis, and L. R. Pratt, Phys. Rev. Lett. **77**, 4966 (1996).
[64] C. A. Reynolds, P. M. King, and W. G. Richards, Mol. Phys. **72**, 251 (1992).
[65] S. J. Weiner, P. A. Kollman, D. T. Nguyen, and D. A. Case, J. Comput. Chem. **7**, 230 (1986).
[66] R. J. Radmer and P. A. Kollman, J. Comput. Chem. **18**, 902 (1997).